RESEARCH ARTICLE

Resonance Frequency Estimation in Series-to-Series Inductive Power Transfer

ISMAIL ADAM[1], (Member, IEEE), MESHARI D. ALANAZI[2],
SHEROZ KHAN[3], (Life Senior Member, IEEE),
MASHKURI YAACOB[4], (Senior Member, IEEE),
ANIS NURASHIKIN NORDIN[4], (Senior Member, IEEE),
HASMAH MANSOR[4], (Senior Member, IEEE),
AND MOHAMED HADI HABAEBI[4], (Senior Member, IEEE)

[1]British Malaysian Institute, University of Kuala Lumpur, Gombak, Kuala Lumpur, Selangor 53100, Malaysia
[2]Department of Electrical Engineering, College of Engineering, Jouf University, Sakaka 72388, Saudi Arabia
[3]Department of Electrical Engineering, College of Engineering and Information Technology, Onaizah Colleges, Unaizah, Al Qassim 56447, Saudi Arabia
[4]Computer and Electrical Engineering Department, International Islamic University, Gombak, Kuala Lumpur, Selangor 53100, Malaysia

Corresponding author: Meshari D. Alanazi (mdalsayer@ju.edu.sa)

ABSTRACT Inductive Power Transfer (IPT) finds applications in various fields that require episodic rather than continuous power supplies, such as implantable medical devices, consumer electronics, IoT applications, civil structure monitoring, and electric vehicle charging. The efficiency of IPT systems depends on the operating frequency which is determined by the coupling coefficient and is affected by the distance between the transmitting and receiving coils. Therefore, accurate estimation of the coupling coefficient and resonance frequency of the IPT is essential to ensure maximum power transfer. This paper presents a novel yet straightforward method for estimating the series-to-series resonant frequency of Inductive Resonant Power Transfer (IRPT) systems. The proof utilizes post-processed experimental data, combining Total Harmonic Distortion (THD) and RMS voltage (VRMS) values evaluated on the transmitter side and obtained through Fast Fourier Transform (FFT). The research shows that the resonant frequency can be determined by identifying the points of lowest THD and highest VRMS on the transmitting side. The analytical plots are experimentally validated by establishing a transmitter unit with a variable frequency pulse generator to drive a DC-to-AC converter connected to a primary coil and a capacitor. The setup includes a display unit and multiple input switches for manually adjusting frequency settings, as well as activating and deactivating the DC-to-AC converter in 10Hz, 100Hz, and 1kHz frequency steps. The study shows promising results in determining the IPT resonance frequency to maximize power transfer, paving the way for advances in inductive resonant Power Transfer applications, such as move-and-charge Wireless Power Transfer (WPT). The novelty of this study not only lies in the simplicity of the proposed technique but also in its feasibility and applicability to the real world application scenarios. The results of this work have applications in many wireless technologies, including IoT applications.

INDEX TERMS Fast Fourier transform, total harmonic distortion, wireless power transfer, inductive resonant series-to-series WPT, resonance frequency.

I. INTRODUCTION

Advances in Wireless Power Transfer (WPT) technology have enabled key applications such as Bluetooth Low Energy (BLE), Radio Frequency Identification (RFID), ZigBee, and 6LoWPAN, which are essential to realizing the potential of the Internet of Things (IoT). IoT has now a key element in integrating smart devices into diverse environments, including highways and vast deserts, by enabling Human-Machine Interfaces (HMI) that provide natural, intuitive, and direct communication between humans and production lines in smart industries that support decision-making or the

The associate editor coordinating the review of this manuscript and approving it for publication was Kai Song.

execution of tasks assigned. A significant trend has emerged in replacing traditional screens and keyboards with voice command features, driven by the deployment of trillions of devices and sensors that require accessible power, ranging from milliwatts to kilowatts [1]. The simplicity, ease, and safety of inductive power transfer (IPT) have made it widely applicable, especially in fields such as biomedical implants, underwater equipment, electric vehicle (EV) charging, and the emerging area of aerial vehicles (or drones) technology. Drones, in particular, have transformed sectors such as rescue missions, crowd monitoring, and wildlife tracking [2]. However, their effectiveness is often limited by short battery life, prompting the need for improved onboard and none-landing charging methods.

In the context of electric vehicles (EVs), Dynamic Wireless Charging Systems (DWCS) are receiving increasing attention due to their potential to address a range of concerns by enabling efficient charging while in motion. Research into reducing start-up transients through novel frequency modulation techniques, has significantly improved charging efficiency, especially during short charging periods [3]. This is crucial to ensuring the seamless operation of EVs in dynamic environments. In addition, studies on parameter variations within DWCS as a future evolving technique emphasize the importance of optimizing factors such as mutual inductance and resonance frequency to enhance power transfer efficiency and overall system performance [4]. Variations in output power in DWCS, driven by changes in coupling coefficients and load resistance, have prompted researchers to explore different compensation techniques. The choice between Series-Series (SS) and Inductor-Capacitor-Capacitor-Series (LCC-S) compensation methods depends on specific performance requirements, with SS providing higher power but greater fluctuations, while LCC-S provides smoother power transfer. These insights are vital for designing, analyzing and operating DWCS that can adapt to varying operating conditions [5].

Control strategies are essential to maintain the stability and efficiency of DWCS of electric vehicles. Techniques such as Sliding Mode Control (SMC) and Feedback Linearization Control (FLC) have been effectively applied to manage charging current fluctuations and compensate for power drops caused by changes in mutual inductance [6]. These strategies are critical to ensuring stable operation, especially in environments where load conditions and coil alignments are constantly changing. The design and optimization of DWCS components, including management of mutual inductance between transmitter and receiver coils and development of high-power systems, are key to achieving optimal performance [7]. For example, maintaining the mutual inductance within a certain range has been shown to significantly enhance the efficiency of the system. Similarly, the design of a 200 kW DWCS with modular power electronics, with minimal infrastructure costs through modularization and optimized coil configurations has demonstrated the

feasibility of high-power dynamic charging, achieving efficiency levels exceeding 90% [8]. In low and medium power applications, the LCC-S compensation topology has proven effective in maintaining system efficiency despite variations in coupling factors [9]. This approach is especially important in industrial automation and other space-constrained environments where efficient power transfer is crucial.

Another area of interest in DWCS is exploring the load-independent characteristics (LIC) of linear relationship between inputs and outputs [10]. Higher-order compensation methods to maintain constant power transfer for load-independent operating conditions are being studied for future transportation [11]. Achieving constant current and voltage modes within specific frequency ranges has been shown to optimize system stability and efficiency. Advanced control strategies, such as observer-based SMC, are being developed to enhance voltage stability and robustness in the face of complex variable load disturbances such as electromagnetic interference [12]. These strategies leverage extended state observers (ESO) to estimate and compensate for disturbances, leading to improved system performance in challenging environments. Accurate coil position recognition in DWCS is critical for maintaining efficient power transfer [13]. Techniques such as multiple linear regression, combined with auxiliary coils, have been proposed to improve misalignment detection and overall charging efficiency. Optimizing constant voltage output in DWCS through the introduction of relay coils has simplified the primary side structure, reduced component costs, and maintained stable voltage output across varying load conditions [14]. This approach has significant implications for the overall cost-effectiveness and efficiency of DWCS. Metering and charging systems are integral to DWCS operation, particularly in ensuring accurate energy measurement and billing. The integration of identification equipment, watt-hour meters, and onboard units has enabled real-time billing and energy metering, even at high vehicular speeds [15]. Experimental validations have confirmed the effectiveness of these systems in dynamic charging environments.

Implementing soft switching strategies in DWCS reduces power loss and enhance system stability [16]. The dual closed-loop control strategies ensure that inverters operate in a soft switching state throughout the charging process, thus improving power transfer efficiency and overall system stability. The advances in DWCS technology, from innovative control strategies to optimized system design, are paving the way for more efficient and reliable electric vehicle charging solutions. These advances not only enhance the performance of DWCS but also expand their applicability across a wide range of industries and environments [17]. Future research should continue exploring new methods to improve power transfer, improve system stability, and to reduce costs to enhan0ce DWCS capabilities.

In Dynamic Wireless Charging Systems (DWCS), the resonance frequency is a critical factor that significantly

influences power transfer efficiency between the transmitting and receiving coils [18]. Resonance occurs when the inductive and capacitive components of the system are tuned to oscillate at a specific frequency, known as the resonance frequency. At this frequency, the system's impedance is minimized, allowing maximum power transfer from the source to the load. The resonance frequency in such a system is determined by the inductance (L) of the coils and the capacitance (C) in the circuit, according to the formula $fr = 1/(2\pi \sqrt{LC})$.

Mutual inductance, which measures how effectively the magnetic field generated by the transmitting coil induces a current in the receiving coil, is vital in this context. In DWCS, mutual inductance is dynamic and varies as the relative position of the coil changes, particularly when the vehicle is in motion demanding the design of a self-tuning controller [19]. This variation affects the coupling coefficient (k), which is directly related to mutual inductance, and consequently impacts the circuit's overall inductance for critical industrial and automotive applications [20]. Since resonance frequency depends on inductance, any change in mutual inductance can shift the system's resonance frequency. For instance, an increase in mutual inductance may lower the resonance frequency, while a decrease might raise it.

The efficiency of power transfer in DWCS is at its peak when the system operates at its resonance frequency by measuring impedance for a relationship between the reflected impedance and the transmission distance [21], [22]. However, changes in mutual inductance can cause the resonance frequency to shift, leading the system to operate off-resonance. This detuning can result in several detrimental effects, including increased impedance, reduced output power, and higher system losses, which manifest as heat and potential damage to system components. For example, if mutual inductance decreases significantly due to coil misalignment or increased distance, the resonance frequency might increase, causing the system to become less efficient in transferring power. Conversely, if mutual inductance increases beyond expected levels, it could lower the resonance frequency, similarly detuning the system.

To manage these changes in the mutual inductance and maintain optimal operation, DWCS often incorporates dynamic tuning mechanisms and advanced control strategies. These include real-time adjustments to capacitance or inductance to keep the system resonant, feedback control systems that adjust operating parameters based on real-time data, and compensation topologies like Series-Series (SS) or LCC-S networks that help stabilize the system's resonance frequency across different conditions [23]. Maintaining resonance through these techniques is essential for the reliable and efficient operation of DWCS, particularly in applications like electric vehicles, where consistent and high-efficiency power transfer is crucial.

To address these challenges, the concept of Inductive Power Transfer (IPT) is explored, focusing on the Series-to-Series Inductive Resonant Power Transfer (IRPT) system. This system features a configuration where a capacitor and

a transmitting coil at the transmission end are connected via inductive coupling to a receiving coil in series with a capacitor at the receiving end to analyze how resonance influences power transfer efficiency from the source to constant loads. The study ultimately shifts focus to exploring the use of FFT for estimating the resonant frequency.
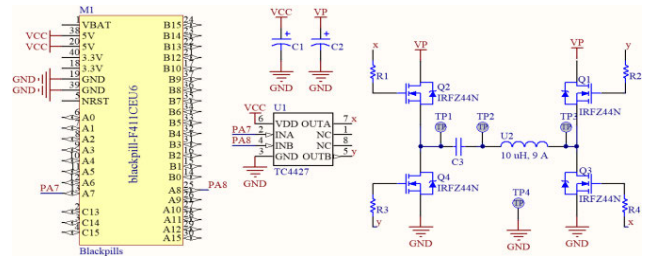

FIGURE 1. The transmitting circuit of the series-to-series inductive resonant wireless power transfer system.

A DC-to-AC inverter that powers the WPT (Wireless Power Transfer) transmitter capacitor and the primary coil is controlled by a variable frequency square wave generator, as depicted in Figure 1. The microcontroller generates a Pulse Width Modulation (PWM) signal with adjustable duration or frequency, maintaining a fixed 50% duty cycle. This PWM signal is then fed into the DC-to-AC inverter, which is configured as an H-bridge driver, through a low-to-high MOSFET driver. The load, consisting of the coil (U2) and capacitor (C3), is connected between the two arms of the H-bridge driver.
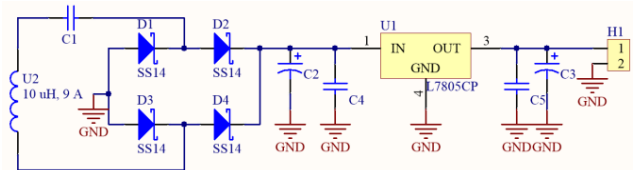

FIGURE 2. The receiving circuit of the series-to-series inductive resonant wireless power transfer system.

On the receiving side, as illustrated in Figure 2, the coil (U2) is connected in series with a capacitor (C1) to create a resonant circuit that captures the transmitted power and delivers it to the load. The output voltage, which is alternating current (AC), is often converted to direct current (DC) for applications such as battery charging. By comparing the circuits in Figures 1 and 2, it is evident that the series-to-series inductive resonant wireless power transfer (SSIRWPT) system acts as a square wave filter. This filter allows signals of the desired frequency to pass to the load while rejecting undesirable frequencies. Consequently, power is transferred to the load wirelessly, without the need for physical connections.

The magnetic linked circuit of the SSIRWPT, illustrated in Figure 3, is mathematically modeled to determine the circuit's transfer function. Equation (1), as shown at the bottom of the next page, provides the circuit transfer function, which
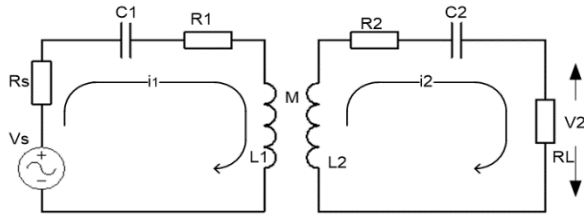
FIGURE 3. The magnetically coupled circuit of the series-to-series inductive resonant wireless power transfer system.

allows for further analysis of the circuit's response at various frequencies.

The frequency response of a circuit can be conveniently analyzed using MATLAB software tools. By employing the transfer function described in equation (1), the circuit's behavior across various frequencies can be visualized, as shown in Figure 4. The magnitude response of the SSIR-WPT shows that the inductive resonant Series-to-Series WPT operates as a bandpass filter. At lower frequencies, it experiences a roll-off of nearly 40 dB per decade, while at higher frequencies, the roll-off is about 20 dB per decade.

The mutual inductance changes with the distance between the coils. As shown in equation (2), increasing the distance between the two coils reduces the coupling coefficient, which in turn decreases the mutual inductance.

$$M = k\sqrt{L_1 L_2} \tag{2}$$

However, it is important to consider the real or effective secondary inductance, defined as the actual secondary inductance (L2e) that influences the circuit's operation. This effective secondary inductance depends on the distance between the transmitter and the receiving coil and can be calculated using equation (3).

$$L_{2e} = L_1 - M^2/L_2 \tag{3}$$

The simulation has been conducted for four different coupling coefficients—0.9, 0.6, 0.3, and 0.1—to illustrate how the circuit's resonance frequency shifts with varying coupling coefficients and, consequently, with distance. Figure 5 displays the circuit's frequency response at these four distinct coupling coefficients: 0.9, 0.6, 0.3, and 0.1.

It is evident from the figure that as the distance between the transmitting and receiving coils increases, the circuit's resonance frequency also increases. The frequency shift is observed, ranging from approximately 50 kHz at a coupling coefficient of 0.9 to about 70 kHz at a coupling coefficient of 0.1. This indicates that to effectively extract power transmitted from the transmitter coil, specific procedures for

accurately estimating the circuit's resonance frequency must be implemented.

A. COUPLING COEFFICIENT AND POWER TRANSFER RELATIONSHIP

The power transfer efficiency (η) of series-to-series inductive resonant wireless power transfer is presented in equation (4), as shown at the bottom of the next page.

Note that R_s and R_L are the source and load impedances, C_1 and C_2 are the capacitors on the transmitting and receiving ends, respectively. R_1 and L_1 represent the resistance and inductance of the transmitting side, while R_2 and L_2 represent the resistance and inductance of the receiving side, k is the coupling coefficient.

Using equation (4) and assuming all parameters except the coupling coefficient are constant, the maximum power efficiency is achieved with a coupling coefficient value of 1. As the coupling coefficient decreases, power efficiency drops exponentially until it reaches zero. In [24], we demonstrated the response of various inductive resonance WPT topologies to changes in the coupling coefficient, which is illustrated in Figure 6.

B. RESONANT FREQUENCY AND POWER TRANSFER RELATIONSHIP

At the resonance frequencies, the circuit seems to be entirely resistive since the capacitive and inductive reactance cancel each other completely at the resonance frequency, in which the power transfer equation is written as in equation (5). Note that ω_0 represents the resonant angular frequency, which equals $2\pi f_0$

$$\eta = \frac{\omega_0^2 \left(k\sqrt{(L_1 L_2)}\right)^2 R_L}{(R_2 + R_L)\left((R_s + R_1)(R_2 + R_L) + \omega_0^2 \left(k\sqrt{(L_1 L_2)}\right)^2\right)} \tag{5}$$

When the reactive components counteract each other at the resonance frequency, the power transfer efficiency reaches its highest level. Consequently, in many publications related to wireless power transfer applications [25], [26], the resonance frequency at the transmitting side and the resonance frequency at the receiving side are determined by,

$$f_x = \frac{1}{2\pi \sqrt{L_x C_x}} \tag{6}$$

Here, the subscript x denotes the transmitting side when it is 1 and the receiving side when it is 2. In various wireless power transfer applications, the operating frequency is typically set to the resonant frequency using equation (6). For example, in wireless phone chargers [27], the operating

$$\frac{V_2(s)}{V_s(s)} = \frac{M s^3 R_2}{(L_1 L_2 + M^2) s^4 + (L_1 R_2 + L_2 R_1) s^3 + \left(R_1 R_2 + \frac{L_2}{C_1} + \frac{L_1}{C_2}\right) s^2 + \left(\frac{R_1}{C_2} + \frac{R_2}{C_1}\right) s + \frac{1}{C_1 C_2}} \tag{1}$$
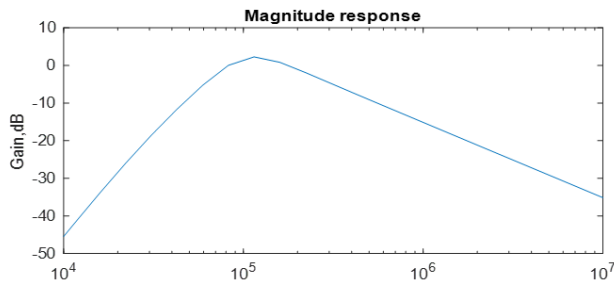
FIGURE 4. The frequency response of the series-to-series inductive resonant wireless power transfer system.
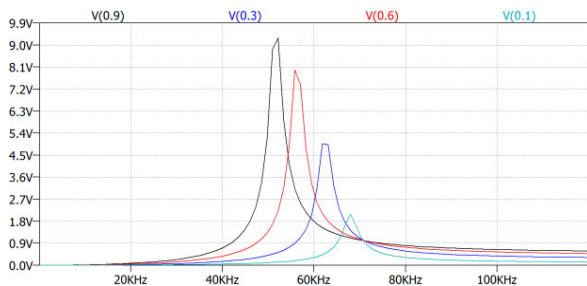

FIGURE 5. Frequency response of series-to-series inductively resonant wireless power transmission at four distinct coupling coefficients.
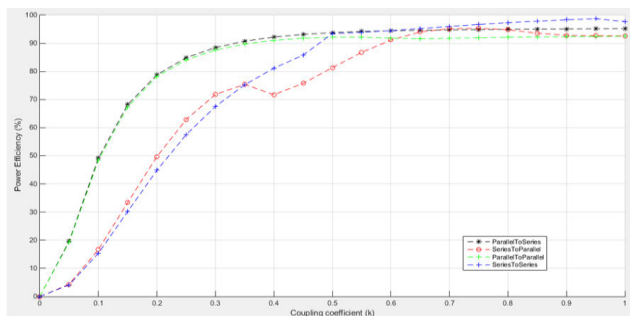

FIGURE 6. The power transfer efficiency of four common inductive resonant wireless power transfer topologies is plotted versus the coupling coefficient (k).

frequency is determined by the physical size of the inductor and capacitor at both the transmission and receiving sides. However, it has been observed that the circuit's input impedance significantly impacts the resonance frequency. The coupling coefficient (k), which is influenced by the separation between the transmitter and receiver, determines the circuit impedance.

$$Z_{in} = R_S + R_1 - j\frac{1}{\omega C_1} + j\omega L_1$$
$$+ \frac{\omega^2 \left(k\sqrt{(L_1 L_2)}\right)^2}{(R_2 + R_L) + j\left(\omega L_2 - \frac{1}{\omega C_2}\right)} \quad (7)$$

The circuit impedance for the circuit shown in Figure 3 is derived in equation (7). Analyzing this equation reveals that the circuit input impedance is directly proportional to the coupling coefficient (k). Furthermore, comparing equation (6) with equation (7) indicates that the resonance frequency of the wireless power transfer is inversely proportional to the coupling coefficient. In summary, the equation implies that the circuit's resonant frequency is higher at lower coupling coefficients and lower at higher coupling coefficients.

C. SOME TECHNIQUES TO IMPROVE POWER TRANSFER

In general, it has been demonstrated that power transfer efficiency reaches its peak at the highest coupling coefficient below the resonance frequency, provided that the load and switching conditions remain constant [28]. In loosely coupled inductive applications, particularly in "moving and charging applications," the coupling coefficient varies with the distance between the transmitter and receiver coils [29]. Any change in this distance alters the circuit's impedance, subsequently affecting the circuit's resonance frequency and power transmission efficiency [30], as discussed in sub-section B.

In the field of wireless power transfer, numerous researchers have developed various innovative strategies to mitigate the decline in power transfer efficiency. To maintain system operation at the resonance frequency, one technique involves adjusting the input and/or output side impedance. This includes inserting a matrix capacitor to dynamically match the input and output impedance, ensuring efficient power transfer to the load [31], [32]. Additionally, a novel series/parallel capacitor arrangement has been implemented on the transmitter side to dynamically adjust the circuit impedance. The authors of [32] continuously regulate the tuning of the capacitor matrix to identify the optimal impedance point for varying distances.

Estimating the coupling coefficient of inductive resonant wireless power transfer is a popular research area. As detailed in [33], the author elucidates the relationship between input impedance and the coupling coefficient, along with a method for dynamically estimating the resonant frequency. This technique records and processes the transmitted current and voltage to identify the current frequency resonance through impedance matching, allowing the system to operate at the proper frequency for significant power transfer. In [34], the primary coil and capacitor current are applied to a phase-locked loop circuit (PLL) to maintain the resonant status of the transmitter's resonant tank despite changes in system impedance.

Another key research focus is ensuring effective power transfer to the load through impedance matching. It has been shown that load impedance is crucial for maximizing

$$\eta = \frac{\omega^2 \left(k\sqrt{(L_1 L_2)}\right)^2 R_I}{\left(R_2 + R_I + j\left(\omega L_2 - \frac{1}{\omega C_2}\right)\right)\left(\left(R_2 + R_2 + j\left(\omega L_2 - \frac{1}{\omega C_1}\right)\right)\left(R_2 + R_I + j\left(\omega L_2 - \frac{1}{\omega C_2}\right)\right) + \omega^2 \left(k^{(L_2 L_2)}\right)^2\right)} \quad (4)$$

power transfer efficiency. As demonstrated in [35], effective power transfer to the load occurs when the load impedance is adjusted to the current "effective impedance." Furthermore, incorporating an impedance-matching network has been proven to enhance power transfer efficiency by gradually aligning the operating frequency with the resonant frequency for various air gaps in wireless power transfer technology.

II. RESONANCE FREQUENCY ESTIMATION BY TOTAL HARMONIC DISTORTION

As previously mentioned, the series-to-series (S-S) inductive resonant wireless power transfer (IRWPT) can be likened to a bandpass filter, as indicated in equation (1). When a square-wave signal is applied to the S-S IRWPT, only the signals within the frequency passband are transmitted to the load, while all other signal components are attenuated. This results in the deformation of the originally transmitted signal. This phenomenon can be illustrated by examining the frequency components of a square wave, as depicted in Figure 7.
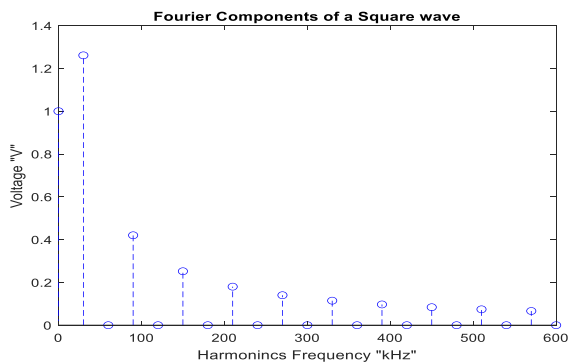

FIGURE 7. The Fourier coefficient of a square wave.

As we know, the Fourier Series allows the decomposition of a supplied square wave into its various frequency components. When the square waveform is symmetrical about the x-axis, the DC component (the first line in Figure 7) is zero. The second line, often referred to as the fundamental component or the first frequency component, represents the signal's fundamental frequency, which usually has the largest magnitude. The presence of other harmonic components depends on the waveform's symmetry around the y-axis. If the waveform is symmetric about the y-axis, even harmonics are present; if the waveform is asymmetric about the y-axis, only odd harmonics are present.

By injecting a square wave with a frequency within the pass band of the filter, as illustrated in Figure 8, almost all of the fundamental components pass through. The second harmonic component is slightly attenuated, while the other harmonic components are greatly attenuated. Because the fundamental component dominates the combination of signals that pass through, the resulting signal appears almost as sine waves at the fundamental frequency, as shown in Figure 9.
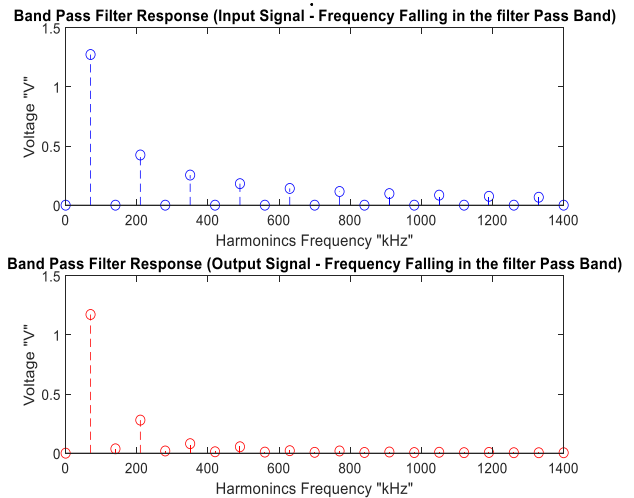

FIGURE 8. The frequency domain looks at the signal generated by passing a square wave with a frequency falling in the pass band of the bandpass filter.
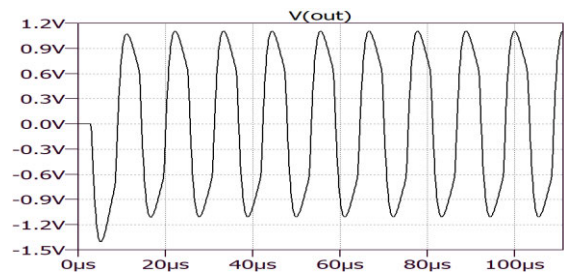

FIGURE 9. The time-domain representation of the signal produced by transmitting a square wave with a frequency within the passband of a bandpass filter.

On the other hand, as demonstrated in Figure 10, injecting a square wave below the passband frequency of the filter causes the fundamental harmonic component to be significantly distorted, the second harmonic component to be slightly distorted, and the higher harmonic components to also be distorted.
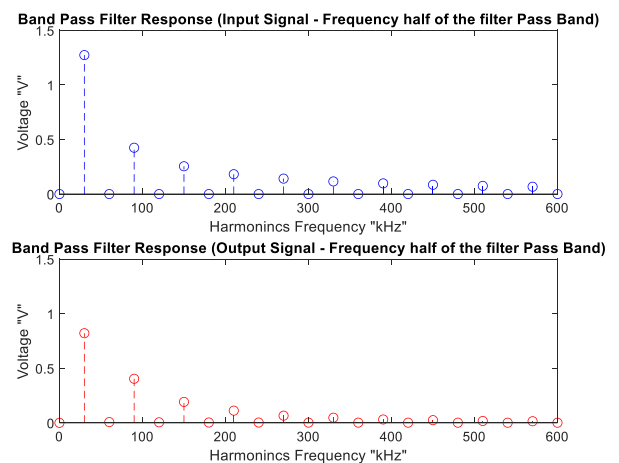

FIGURE 10. The frequency-domain representation of the signal generated by transmitting a square wave with a frequency within the passband of a bandpass filter.

As a result, when the square wave signal is passed through the bandpass filter, it will appear distorted, as shown in Figure 11. The fundamental frequency of the signal displays some distortion, whereas the higher frequency components, like the second and third harmonics, remain largely undistorted.
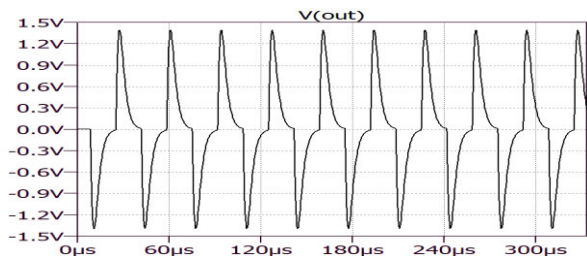

FIGURE 11. The time-domain representation of the signal generated by transmitting a square wave with a frequency below the passband of a bandpass filter.

Meanwhile, the fundamental harmonic component, the second harmonic component, and the third harmonic component are all slightly distorted when a square wave with a frequency above the bandpass filter's passband is injected into the filter, as shown in Figure 12. However, all higher harmonic components are greatly attenuated.
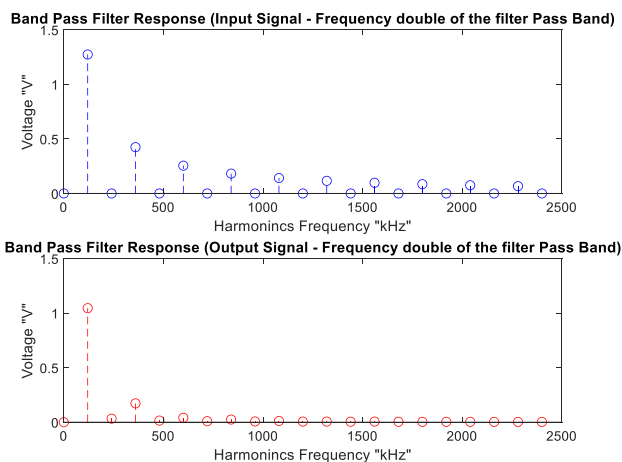

FIGURE 12. The frequency-domain representation of the signal produced by transmitting a square wave with a frequency above the passband of a bandpass filter.

Due to the significant distortion at higher frequency components, the square wave signal transforms into a distorted square wave at the fundamental frequency, as shown in Figure 13.

According to [36], the total harmonic distortion (THD) of a signal can be calculated by dividing the sum of the squares of the higher harmonic components (s_x) by the square of the fundamental component (s_1). Here, s_1 represents the fundamental component, and s_x represents the harmonic components greater than the fundamental component,
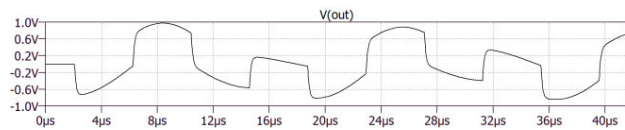

FIGURE 13. The time-domain representation of the signal produced by transmitting a square wave with a frequency above the passband of a bandpass filter.

as shown in equation (8).

$$THD_s = \frac{s_2^2 + s_3^2 + \dots\dots + s_n^2}{s_1^2} \qquad (8)$$

Therefore, by referring to the graphical representation of the signal in the frequency domain as it passes through the bandpass filter in Figures 8, 10, and 12, the THD of a square wave with a frequency in the passband of the filter will be at its lowest. This is because the filter allows the fundamental frequency to pass while proportionally reducing all other harmonic components. Meanwhile, the THD of a square wave with a frequency either higher or lower than the bandpass filter's passband will be higher, as the fundamental component experiences more distortion than the other harmonics, as shown in Figures 10 and 12.

Therefore, this study suggests using the total harmonic distortion (THD) parameter to determine the resonance frequency of the series-to-series (SS) WPT inductive resonance by analyzing the signal at the transmitter side. In the transmitter, the signal is sampled and processed for its Fourier components using the Fast Fourier Transform (FFT), and the THD is calculated to estimate the resonance frequency or operating frequency of a square wave at the input.

III. THE CIRCUIT SIMULATION

In this study, we simulate the T-equivalent circuit of the SS WPT inductive resonance, derived from Figure 3 and depicted in Figure 14, using a square wave with frequencies below, within, and above the passband frequency of the T-network. In this simulation, the coupling coefficient is set to 0.6, resulting in a mutual inductance (M) of 6 μH and a secondary inductance (L2) of 6.4 μH. The dynamic values of mutual inductance and secondary inductance are calculated based on the definitions provided in [24]. These values are determined using equations (2) and (3), which have been reformulated in this paper.

The simulations are conducted for square waves with frequencies of 30kHz, 55kHz, and 120kHz. By setting the square wave input to a 50% duty cycle with an input voltage of 1Vp-p, the output waveforms for all steps are recorded and presented in Figure 15.

To enhance visibility, the 5-cycle plot of each signal shown in Figure 15 is duplicated and displayed in Figure 16. The signal is replotted to offer a clearer representation for further analysis.

Using the Fourier transform option, the circuit response is simulated in the frequency domain at all three frequencies
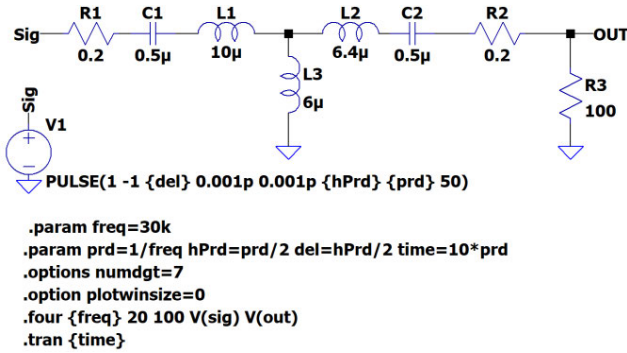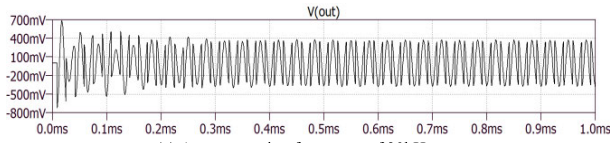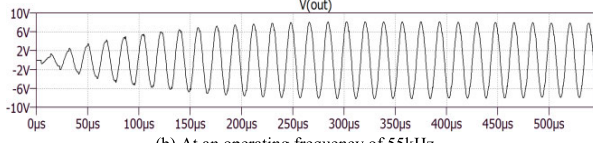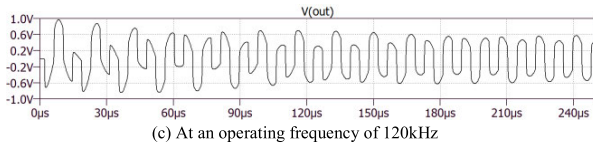
FIGURE 14. T-equivalent circuit of the series-to-series inductive resonant wireless power transfer at a coupling coefficient of 0.6.

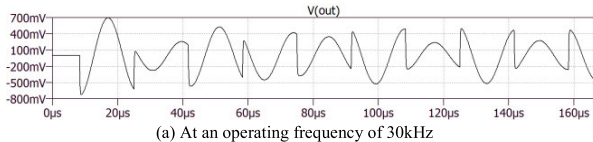(a) At an operating frequency of 30kHz
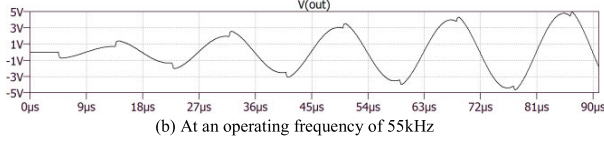
(b) At an operating frequency of 55kHz
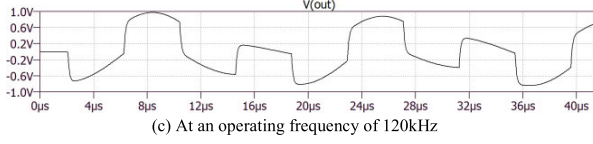
(c) At an operating frequency of 120kHz

FIGURE 15. Thirty cycles of the output signal at various operating frequencies at the 'Out' point of Figure 14.

(a) At an operating frequency of 30kHz

(b) At an operating frequency of 55kHz

(c) At an operating frequency of 120kHz

FIGURE 16. Five cycles of the output signal at various operating frequencies at the 'Out' point of Figure 14.

(30 kHz, 70 kHz, and 120 kHz), with only the first 20 harmonic components recorded for each signal frequency. Figures 17 to 19 display the Fourier components of the input and output signals for all simulations performed. To facilitate

comparison, the input and output signals are stacked against each other.
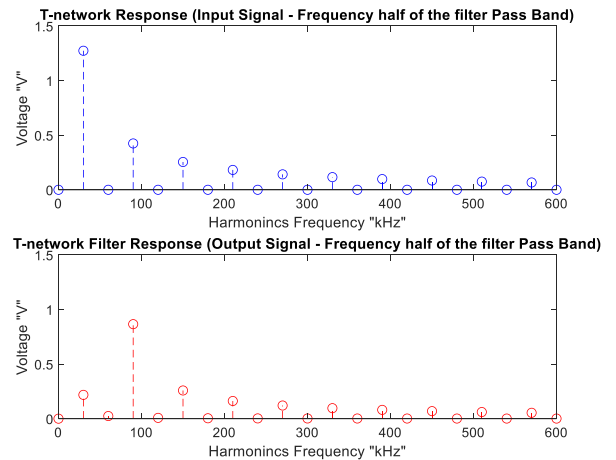

FIGURE 17. The frequency-domain re-presentation of the signal at 30kHz.
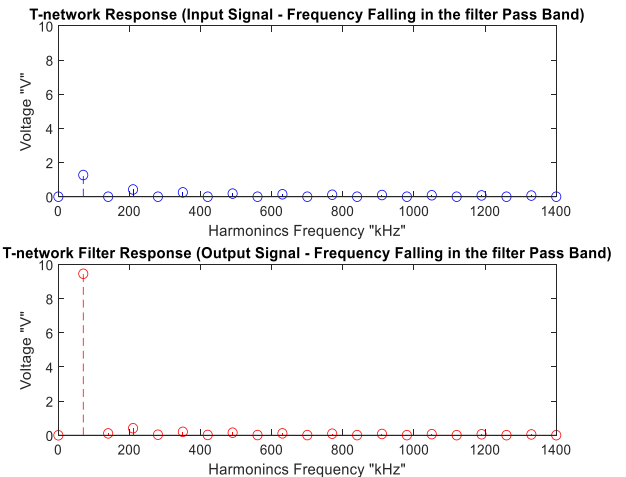

FIGURE 18. The frequency-domain re-presentation of the signal at 70kHz.
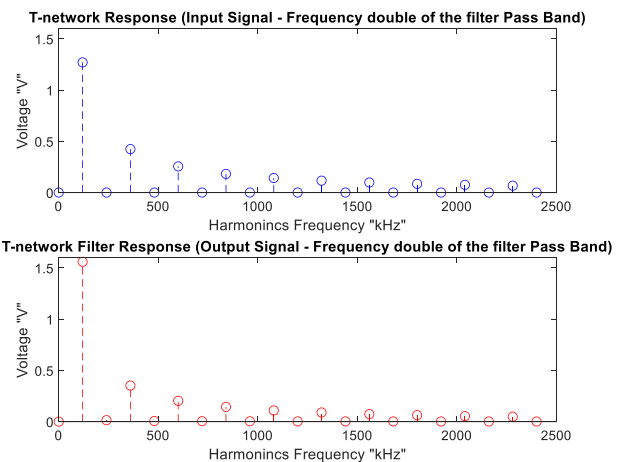

FIGURE 19. The frequency-domain re-presentation of the signal at 120kHz.

Table 1 presents the Total Harmonic Distortion (THD) at all simulated frequencies. As anticipated, the signal

within the T-network's passband exhibits the lowest level of distortion.

TABLE 1. The values of THD at various frequency.

Frequency (kHz)	THD
30.00	431.184151%
70.00	5.659976%
120.00	30.191237%

The simulation results corroborate the findings described in Part II: when the operating frequency is close to or within the passband frequency of the bandpass filter, as illustrated in Figure 18, the filtered signal is primarily dominated by the fundamental frequency. Conversely, at higher or lower frequencies, as shown in Figures 17 and 19, the fundamental frequency becomes less dominant. These results support the hypothesis that the resonant frequency of the inductively resonant series-to-series WPT can potentially be estimated through Total Harmonic Distortion (THD) analysis.

IV. EXPERIMENTAL SETUP

Figure 20 illustrates the experimental setup designed to evaluate the proposed resonance frequency estimation of the series-to-series inductive resonance wireless power transfer. The transmitter unit is mounted on a linear rail, allowing the receiver to move back and forth freely along the rail. The transmitter unit is equipped with a variable frequency Pulse Width Modulation (PWM) generator to drive a DC-to-AC converter, which is connected to a primary coil and capacitor. Additionally, the setup includes a display unit and multiple input switches for manual frequency adjustments, as well as for activating and deactivating the DC-to-AC converter.
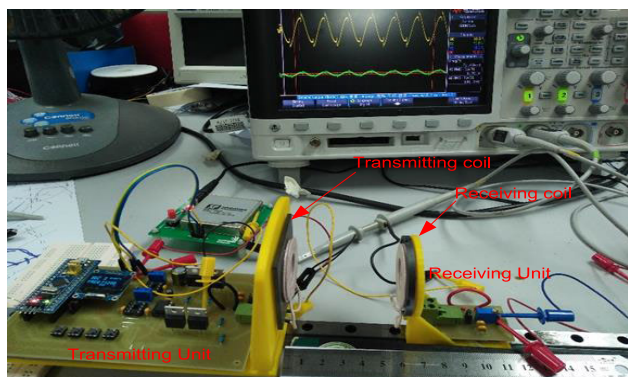

FIGURE 20. The experimental set-up of the project.

The display unit shown in Figure 21 is used to indicate the current frequency, the activation state of the PWM generator, and the selected frequency. The frequency step sizes are represented by 0, 1, and 2, corresponding to step increments of 10 Hz, 100 Hz, and 1 kHz, respectively.

The receiver unit comprises a secondary coil and a capacitor to feed the load resistor through multiple resistive connections. The distance between the transmitting and
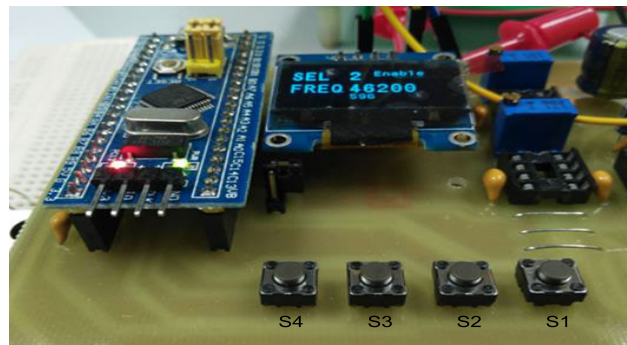

FIGURE 21. A closer look at the transmitter side.

receiving units is measured using a ruler that is permanently mounted on the railing mechanism.

The signal is recorded on both the transmitter and receiver sides to evaluate the resonance frequency estimation. Measurements are specifically taken at the load resistor for the reception signal and across the primary coil for the transmitter signal. A gap of 1.5 cm is established between the transmitter and receiver coils, and the operating frequency on the transmission side is set to 30kHz, 50kHz, 74kHz, 80kHz, 100kHz, and 120kHz. Oscilloscope data for all signal values are recorded for subsequent signal processing. This post-signal processing is conducted using MATLAB software. To obtain THD and VRMS, a fast Fourier transform analysis is performed. The results of the study on the resonance frequency of the series-to-series WPT are presented in Table 2.

TABLE 2. The values of THD and VRMS at respecting frequency.

Frequency (kHz)	THD	V_{RMS}
30.00	7.1502	2.8159
50.00	2.0418	3.9015
70.00	0.5142	8.3224
74.06	0.3662	8.9583
80.00	0.7108	8.0209
100.00	0.9100	5.9962
120.00	1.0294	5.1120

In the second experiment, the frequency at the transmitter was adjusted to match the resonance frequency, and the transmitting and receiving coils were initially positioned 0 cm apart. The operating frequency, which is the period of the inverter's PWM, was manually tuned on the transmitter side to emit a signal that approximates a sine wave. This tuning ensures the operating frequency is set to the resonance frequency appropriate for the given distance between coils. The receiving coil was then gradually moved away from the transmitting coil in 1 cm increments, up to a maximum distance of 5 cm. At each distance, the resonance frequency and output voltages were recorded and documented in Table 3, detailing how each adjustment in the spacing between the transmitter and receiver coils impacted performance.

TABLE 3. Output voltage at resonance frequency versus coil distance.

Distance (cm)	Frequency (Hz)	V_{RMS} at resonance
0	58480	9.96
1	71720	4.24
2	74180	1.42
3	75740	0.644
4	75860	0.325
5	76220	0.172

Finally, in the last experiment, the frequency on the transmitter side was adjusted to 55 kHz and 65 kHz, with the transmitter and receiver coils of the inductively resonant WPT connection aligned at a distance of 0 cm. The received voltage is measured at the receiving coil and recorded in Table 4. Similar to the previous experiment, the receiver coil was moved in 1 cm increments up to a distance of 5 cm. Again, the received voltage is measured and appropriately recorded in Table 4.

TABLE 4. Output voltage at different operating frequency and coil distance.

	V_{RMS} (across 100 Ω loads)	
Distance (cm)	At 55kHz	At 65kHz
0	8.8	7.73
1	2.07	3.46
2	0.650	1.06
3	0.300	0.337
4	0.154	0.238
5	0.069	0.124

V. RESULTS AND DISCUSSION

Figure 22 illustrates a sample of the signal recorded during the experiment, showcasing three different operating frequencies: 30 kHz, 60 kHz, and 120 kHz. The distance between the transmitter and receiver coils in this example is 1 cm.
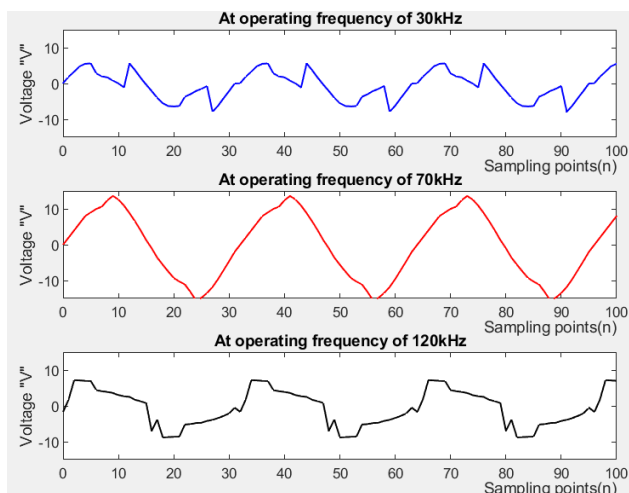

FIGURE 22. Example of an output signal measured on a load with three distinct operating frequencies, with the coils positioned 1 cm apart.

To calculate the THD and VRMS values from an FFT, only a single complete cycle of the signal is needed. Consequently,

just a portion of the recorded signal, marked by the red dotted circle in Figure 23, will be analyzed for THD and VRMS.
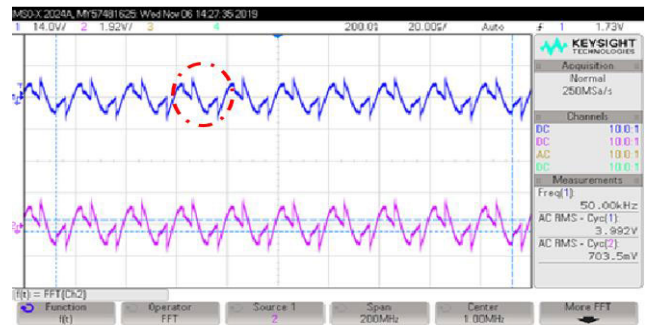

FIGURE 23. Signal transmitted (above) and received (below) at 50kHz.

In this study, a single complete cycle of the signal was interpolated for post-processing, as shown by the red dotted circles in Figure 23 and recreated in Figure 24. For example, in Figure 24, the 32-bit data points are as follows: 0.1, 1.9, 3.3, 4.8, 5.5, 5.6, 2.8, 2, 1.7, 0.8, 0, −1.1, 5.6, 3.7, 1.6, −0.3, −2.1, −4, −5.5, −6.3, −3.7, −3, −2.1, −1.5, −0.7, −7.9, −6.2, −6.5, −6.4, −4.1, −2.1, 0.
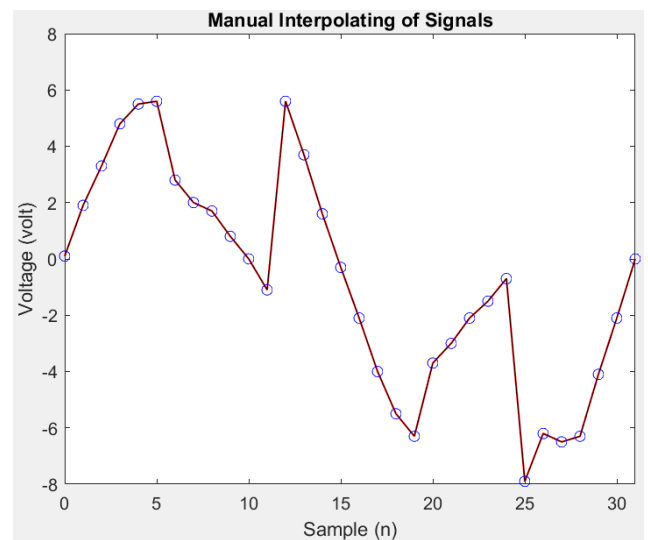
FIGURE 24. Manual interpolating of the recorded signal.

Using the data from the earlier mentioned procedure, a 32-bit Fast Fourier Transform was performed and is illustrated in Figure 25. Additionally, the Fourier components obtained from this transform were employed to calculate the THD and VRMS. This analysis was conducted for each data point across all frequencies, and the results were compiled in Table 2.

Figure 26 displays plots of the received voltage at various operating frequencies and coil distances, based on the data from Tables 3 and 4. A comparison of the received voltage at the resonance frequency with that at two other frequencies shows that the voltage received at the resonance frequency is significantly higher.

FIGURE 25. The FFT of the recorded signal (50kHz).

FIGURE 26. The plot of received voltage against distance for operating frequency at 55kHz, 65kHz, and the resonance frequency.

Using the data from Table 4, the power delivered to the load is calculated by squaring the received voltage, dividing by 100, and recording the results in Table 5.

TABLE 5. Output power at various operating frequency and coils distance.
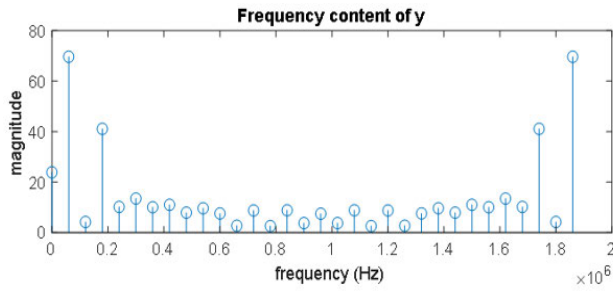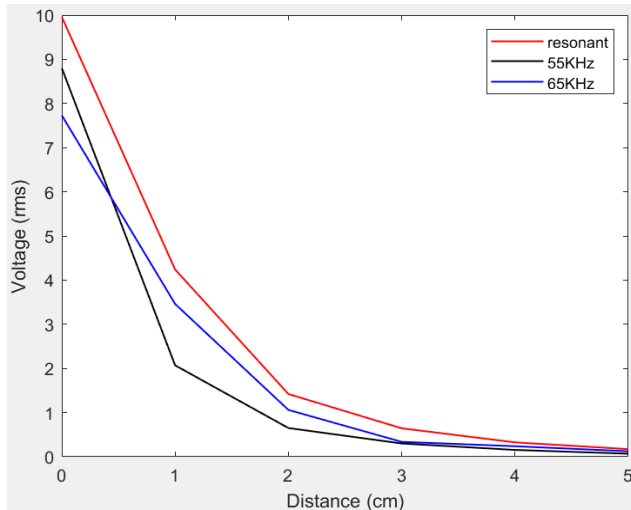
Distance (cm)	At 55kHz	At 65kHz	At resonance
0	0.774400w	0.597529w	0.992016w
1	0.042849w	0.119716w	0.179776w
2	0.004225w	0.011236w	0.020164w
3	0.000900w	0.001136w	0.004147w
4	0.000237w	0.000566w	0.001056w
5	0.000154w	0.000154w	0.000296w

Additionally, using the data from Table 5, a graph of the power received by the load at various operating frequencies and coil separations has been plotted, as shown in Figure 27. Generally, the data shows that the power received at the resonance frequency predominates, particularly at distances less than 2 cm.

The data clearly shows that setting the transmitter's operating frequency—namely, the period of the DC-to-AC inverter PWM—closer to the resonance frequency significantly improves power delivery to the load. For example, at a coil separation of 0 cm, the power transferred to the load is greater at an operating frequency of 55 kHz than at 65 kHz.
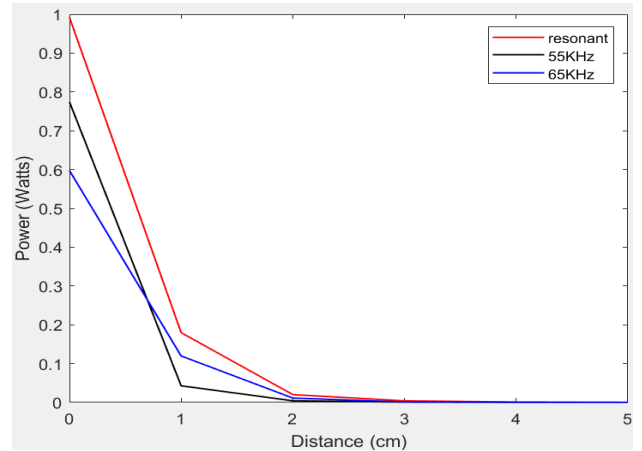
FIGURE 27. The graph shows received power as a function of distance for operating frequencies of 55kHz, 65kHz, and the resonance frequency.

This increase in power is attributed to the 55 kHz frequency being closer to the resonance frequency of 58.48 kHz at this separation. On the other hand, at a coil separation of 1 cm, the power transferred is higher at an operating frequency of 65 kHz compared to 55 kHz, since the 65 kHz frequency is closer to the new resonance frequency of 71.72 kHz.

The performance of power transfer is further analyzed by plotting the power transfer ratio, as illustrated in Figure 28. To aid in analysis, this ratio, comparing power received at the resonance frequency to that received at a fixed frequency, is expressed in percentage terms. The figure clearly shows that power transfer at the resonance frequency is substantially higher than at the fixed frequency, with the magnitude of this increase depending on the distance between the transmitter and receiver coils.

FIGURE 28. The graph displays the ratio of power received at the resonance frequency to the power received at a fixed frequency.

The graph indicates that the power received at the resonant frequency increases with coil distances up to 3 cm, attributed to the resonant frequency enhancing power transfer over this range when power availability is adequate. Beyond 3 cm of

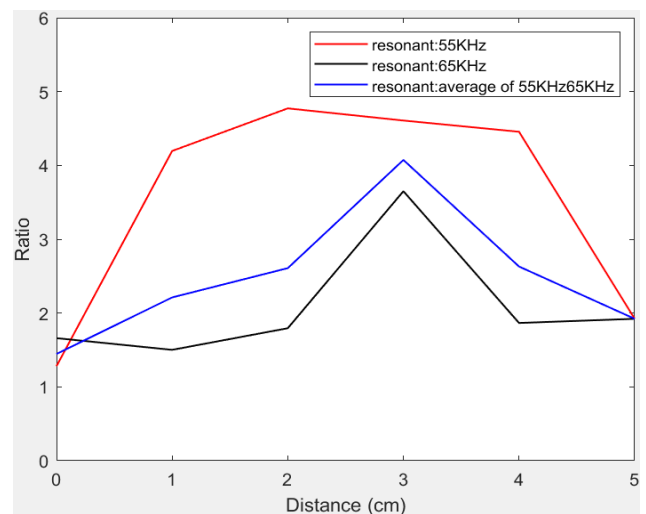coil separation, the ratio of received power begins to fall as the power from the source becomes the crucial factor affecting the transfer. Additionally, the graph highlights that maintaining the operating frequency at the resonance frequency ensures that no less than 50% of the power is conserved.

Ultimately, the data gathered from both simulations and experiments highlighted several key observations, which can be summarized as follows:

1. The simulation outcomes depicted in Figure 16 closely resemble the experimental results shown in Figure 22.
2. At a coil separation of 1.5 cm, the minimum THD is observed at 74.06 kHz, which lies in the center of the tested frequencies (see Table 2).
3. The maximum VRMS received corresponds to the point of lowest THD.
4. As the operating frequency approaches the resonance frequency, the power received increases.

VI. CONCLUSION

This paper presents and validates a direct method for determining the resonance frequency of a series-to-series inductive resonant wireless power transfer (WPT) system, using Total Harmonic Distortion (THD) and Root Mean Square Voltage (VRMS). A transmitting module has been constructed, equipped with a microcontroller-based Pulse Width Modulation (PWM) generator, a DC-to-AC inverter, and a transmitting resonator. The frequency of the PWM generator can be manually adjusted in steps of 10Hz, 100Hz, or 1 kHz, within a range of 20 kHz to 120 kHz. A receiving unit consisting of a receiving resonator and a resistive load, has also been developed. Signals from both the transmitter and receiver were recorded and analyzed.

Analysis of these signals for THD and RMS voltage values, shown in Table 2, have revealed that the highest RMS voltage corresponds to the lowest THD, which indicates that the peak signal occurs at the resonance frequency, demonstrating that THD is an effective tool to determine the resonance frequency of an inductive resonant WPT system. Further evidence of this has been provided by comparing the power transferred at the resonance frequency with the power received at a fixed frequency, as detailed in Table 5. This comparison shows that optimal power transfer in an inductive resonant WPT system is achieved when the transmitter operating frequency matches the resonance frequency.

From a practical standpoint, using THD to estimate the resonance frequency in such systems offers several advantages, including simplified signal measurement. This method only requires voltage measurements at the transmitting coil, unlike the input impedance method which relies on variations in circuit impedance and requires current and voltage measurements. In addition, this technique is not affected by system impedance, making it a simpler alternative.

However, this approach has a drawback: it imposes a high demand on computational resources. The processor must be capable to sample the transmitted signal at rates significantly higher than the operating frequency (8 or 16 times) and efficiently handle complex computations involving FFT, THD, and VRMS within the given processing time. To avoid aliasing effects, it is recommended to oversample the signal. Modern processors such as ARM Cortex-M, designed specifically for microcontroller applications, are well-suited to this task. These processors feature multiple cores, high clock speeds, and advanced instruction sets, which greatly enhance their data processing capabilities. These features allow these processors to achieve high processing speeds, manage large volumes of data, and process extensive data streams efficiently, as well as perform tasks such as signal sampling, FFT computations, and other real-time data processing operations effectively.

The results of this research indicate potential paths for future studies aiming at automated and practical regulation of the WPT resonance frequency, such as using an Artificial Neural Network (ANN)-based method that requires real-time training and validation. The resonance frequency estimation technique explored here is currently being evaluated for its suitability in wireless power transfer technologies involving simultaneous movement and charging. This paper presents and validates a straightforward method for determining the resonance frequency of a series-to-series inductive resonant wireless power transfer (WPT) system, using THD (Total Harmonic Distortion) and VRMS (Root Mean Square Voltage). A transmitter module has been constructed, equipped with a microcontroller-based PWM (Pulse Width Modulation) generator, a DC-to-AC inverter, and a transmitting resonator. The frequency of the PWM generator can be manually adjusted in steps of 10Hz, 100Hz, or 1 kHz, within a range of 20 kHz to 120k Hz. A receiver unit, consisting of a receiving resonator and a resistive load, has been also developed. Signals from both the transmitter and receiver have been recorded and analyzed.

Analysis of these signals for THD and RMS voltage, shown in Table 2, has revealed that the highest RMS voltage corresponds to the lowest THD. This indicates that the peak signal occurs at the resonance frequency, which demonstrates that THD is an effective tool to determine the resonance frequency of the inductive resonant WPT system. Additional evidence for this was provided by comparing the transferred power at the resonance frequency with the received power at a fixed frequency, as detailed in Table 5. This comparison shows that optimal power transfer in an inductive resonant WPT system is achieved when the transmitter operating frequency matches the resonance frequency.

From a practical standpoint, using THD to estimate the resonance frequency in such systems offers several advantages, including simplified signal measurement. This method only requires voltage measurements at the transmitting coil, unlike the input impedance method which relies on variations in circuit impedance and requires current and voltage measurements. In addition, system impedance does not affect this technique, making it a simpler alternative.

However, this approach has a drawback: it imposes a high demand on computational resources. The processor must be able to sample the transmitted signal at rates well above the operating frequency (8 or 16 times) and efficiently handle complex computations involving FFT, THD, and VRMS within the designated processing time. To avoid aliasing effects, it is recommended oversample the signal. Modern processors like the ARM Cortex-M, designed specifically for microcontroller applications, are well-suited to this task. These processors feature multiple cores, high clock speeds, and advanced instruction sets, which significantly enhance their data processing capabilities. Such features allow these processors to achieve high processing speeds, manage large amounts of data, and process extensive data streams efficiently, as well as perform tasks such as signal sampling, FFT computations, and other real-time data processing operations effectively.

The results of this research indicate potential paths for future studies aiming at the automated and practical regulation of the WPT resonance frequency, such as using an Artificial Neural Network (ANN)-based method that requires real-time training and validation. The resonance frequency estimation technique explored here is currently being evaluated for its suitability in wireless power transfer technologies involving simultaneous movement and charging.

In summary, the advantages of the proposed technique are outlined in Table 6. Seven key benefits make this technique highly promising for wireless power transfer applications.

TABLE 6. Key advantages of the proposed wireless power transfer technique.

Advantage	Description
Simplicity	The method is straightforward to implement, requiring minimal setup and calibration.
Feasibility	The technique is feasible for real-world applications, especially in wireless power transfer systems for IoT devices.
Applicability	Applicable across a wide range of wireless power transfer technologies, including dynamic charging scenarios.
Effectiveness	Reliably identifies the resonant frequency using Total Harmonic Distortion (THD) and Root Mean Square Voltage (VRMS).
Reduced Complexity	Only requires voltage measurements at the transmitting coil, reducing the complexity compared to impedance-based methods.
Independence from System Impedance	Not affected by variations in system impedance, making it more robust and easier to apply in various conditions.
Potential for Automation	Can be adapted for automated resonance frequency regulation using techniques like Artificial Neural Networks (ANNs).

REFERENCES

[1] F. Longo and A. Padovano, "Voice-enabled assistants of the operator 4.0 in the social smart factory: Prospective role and challenges for an advanced human–machine interaction," *Manuf. Lett.*, vol. 26, pp. 12–16, Oct. 2020.

[2] O. Allama, M. H. Habaebi, S. Khan, M. R. Islam, and A. Alghaihab, "Simulation and control design of a midrange WPT charging system for in-flight drones," *Energies*, vol. 16, no. 15, p. 5746, Aug. 2023.

[3] K. K. Prasad and V. Agarwal, "A novel frequency modulation technique to minimize the start-up transients in dynamic wireless charging systems for electric vehicles," in *Proc. Wireless Power Week (WPW)*, Jul. 2022, pp. 834–838.

[4] K. Kumar, K. V. V. S. R. Chowdary, B. Nayak, and V. Mali, "A study on the implications of parameter variation involved with dynamic wireless charging system for vehicular application," in *Proc. IECON 49th Annu. Conf. IEEE Ind. Electron. Soc.*, Oct. 2023, pp. 1–5.

[5] K. Kumar, V. V. S. R. Chowdary, V. Mali, and R. Kumar, "Analysis of output power variation in dynamic wireless charging system for electric vehicles," in *Proc. IEEE 2nd Int. Conf. Smart Technol. Power, Energy Control (STPEC)*, Dec. 2021, pp. 1–6.

[6] W. Zhang, X. Fan, Y. Zheng, and X. Zhang, "Application of sliding mode control with leakage loop modulation in dynamic wireless charging system of electric vehicle," in *Proc. 12th Int. Symp. Comput. Intell. Design (ISCID)*, vol. 1, Dec. 2019, pp. 262–265.

[7] K. V. V. S. R. Chowdary and K. Kumar, "Assessment of dynamic wireless charging system with the variation in mutual inductance," in *Proc. IEEE 19th India Council Int. Conf. (INDICON)*, Nov. 2022, pp. 1–4.

[8] L. Xue, V. Galigekere, G.-J. Su, R. Zeng, M. Mohammad, E. Gurpinar, S. Chowdhury, and O. Onar, "Design and analysis of a 200 kW dynamic wireless charging system for electric vehicles," in *Proc. IEEE Appl. Power Electron. Conf. Expo. (APEC)*, Mar. 2022, pp. 1096–1103.

[9] M. Zavrel, V. Kindl, and M. Tyrpekl, "Dynamic wireless charging using LCC-S compensation topology in low and medium power applications," in *Proc. IEEE 32nd Int. Symp. Ind. Electron. (ISIE)*, Jun. 2023, pp. 1–6.

[10] Z. Zhou, Z. Liu, H. Su, and L. Zhang, "Feedback linearization control for the receiving-side buck converter of dynamic wireless charging system of electric vehicles," in *Proc. IECON 47th Annu. Conf. IEEE Ind. Electron. Soc.*, Oct. 2021, pp. 1–6.

[11] K. V. V. S. R. Chowdary, K. Kumar, R. K. Behera, S. Banerjee, and R. R. Kumar, "Load independent characteristics of dynamic wireless charging system through higher order compensation," in *Proc. IEEE Int. Conf. Power Electron., Drives Energy Syst. (PEDES)*, Dec. 2020, pp. 1–6.

[12] J. Yue, Z. Liu, Z. Jiang, D. Chen, and H. Su, "Observer-based SMC for dynamic wireless charging system of electric vehicles with complex disturbances," in *Proc. 18th IEEE Conf. Ind. Electron. Appl. (ICIEA)*, Aug. 2023, pp. 1139–1144.

[13] X. Xue, Z. Liu, J. Liu, W. Chen, M. Zhang, and J. Yue, "Recognition of coil position information in dynamic wireless charging system based on multiple linear regression," in *Proc. IECON (Ind. Electron. Conf.)*, 2023, pp. 1–5.

[14] Y. Jia, X. Li, L. Sang, and K. Wang, "Research on constant voltage output optimization method for EV dynamic wireless charging system," in *Proc. 8th Int. Conf. Power Electron. Syst. Appl. (PESA)*, Dec. 2020, pp. 1–4.

[15] Z. Danping, L. juan, C. Yuchun, L. Yuhang, and C. Zhongjian, "Research on electric energy metering and charging system for dynamic wireless charging of electric vehicle," in *Proc. 4th Int. Conf. Intell. Transp. Eng. (ICITE)*, Sep. 2019, pp. 252–255.

[16] R. Long, L. Zhang, and Q. Chen, "Soft switching strategy of dynamic wireless charging system for electric vehicles," in *Proc. 33rd Youth Academic Annu. Conf. Chin. Assoc. Autom. (YAC)*, May 2018, pp. 738–742.

[17] J. He, Y. Chen, J. Lin, J. Chen, L. Cheng, and Y. Wang, "Review of modeling, modulation, and control strategies for the dual-active-bridge DC/DC converter," *Energies*, vol. 16, no. 18, p. 6646, Sep. 2023.

[18] C. Degen, "Inductive coupling for wireless power transfer and near-field communication," *EURASIP J. Wireless Commun. Netw.*, vol. 2021, no. 1, pp. 1687–1499, 2021.

[19] M. Moghaddami, A. Sundararajan, and A. I. Sarwat, "A power-frequency controller with resonance frequency tracking capability for inductive power transfer systems," *IEEE Trans. Ind. Appl.*, vol. 54, no. 2, pp. 1773–1783, Mar. 2018.

[20] S. Schaecher. (2018). *Infineon White Paper Resonant Wireless Power Transfer*. [Online]. Available: www.infineon.com/wirelesscharging

[21] J. Bing, T. Longzhao, Y. Zihao, W. Lieyue, and L. Guorong, "A novel distance measurement method based on reflected impedance for resonant wireless power transmission system," in *Proc. Asia Energy Electr. Eng. Symp. (AEEES)*, May 2020, pp. 1–5.

[22] H. Allamehzadeh, "Wireless power transfer (WPT) fundamentals with resonant frequency-dependent parameters, energy transfer efficiency, and green technology applications," in *Proc. IEEE 48th Photovoltaic Spec. Conf. (PVSC)*, Jun. 2021, pp. 0036–0040.

[23] N. Y. Kim, K. Y. Kim, J. Choi, and C.-W. Kim, "Adaptive frequency with power-level tracking system for efficient magnetic resonance wireless power transfer," *Electron. Lett.*, vol. 48, no. 8, p. 452, 2012.

[24] I. Adam, K. A. Kadir, S. Khan, A. Nurashikin, and H. Mansor, "Inductive resonant power transfer and topology consideration," in *Proc. IEEE 3rd Int. Conf. Eng. Technol. Social Sci. (ICETSS)*, Aug. 2017, pp. 1–5.

[25] Y. Zhang, T. Lu, Z. Zhao, F. He, K. Chen, and L. Yuan, "Selective wireless power transfer to multiple loads using receivers of different resonant frequencies," *IEEE Trans. Power Electron.*, vol. 30, no. 11, pp. 6001–6005, Nov. 2015.

[26] X. Dai, X. Li, Y. Li, P. Deng, and C. Tang, "A maximum power transfer tracking method for WPT systems with coupling coefficient identification considering two-value problem," *Energies*, vol. 10, no. 10, p. 1665, Oct. 2017.

[27] C.-G. Kim, D.-H. Seo, J.-S. You, J.-H. Park, and B. H. Cho, "Design of a contactless battery charger for cellular phone," *IEEE Trans. Ind. Electron.*, vol. 48, no. 6, pp. 1238–1247, Dec. 2001.

[28] I. Adam, S. Khan, Z. Zaharuddin, K. A. Kader, F. D. A. Rahman, A. N. Nordin, N. A. C. Musa, and M. Yaacob, "Frequency reliant wireless power transfer link for a applications of mWatts devices," in *Proc. 7th Int. Conf. Comput. Commun. Eng. (ICCCE)*, Sep. 2018, pp. 1–5.

[29] Z. Zhang and K. T. Chau, "Homogeneous wireless power transfer for move-and-charge," *IEEE Trans. Power Electron.*, vol. 30, no. 11, pp. 6213–6220, Nov. 2015.

[30] Y. Li, Q. X. Yang, H. Y. Chen, X. Zhang, and L. Jin, "Basic study on improving power of wireless power transfer via magnetic resonance coupling," *Adv. Mater. Res.*, vol. 459, pp. 445–449, Jan. 2012.

[31] D.-W. Seo, J.-H. Lee, and H.-S. Lee, "Optimal coupling to achieve maximum output power in a WPT system," *IEEE Trans. Power Electron.*, vol. 31, no. 6, pp. 3994–3998, Jun. 2016.

[32] X. Dai, X. Li, Y. Li, and A. P. Hu, "Maximum efficiency tracking for wireless power transfer systems with dynamic coupling coefficient estimation," *IEEE Trans. Power Electron.*, vol. 33, no. 6, pp. 5005–5015, Jun. 2018, doi: 10.1109/TPEL.2017.2729083.

[33] I. Adam, S. Khan, Z. Zaharudin, K. A. Kadir, A. N. Nurdin, and M. Yaacob, "An estimation of the coupling coefficient of the series inductive resonant wireless power transfer," *Test Eng. Manag.*, vol. 81, no. 5702, pp. 5756–5791, 2019.

[34] Q. Li and Y. C. Liang, "An inductive power transfer system with a high-Q resonant tank for mobile device charging," *IEEE Trans. Power Electron.*, vol. 30, no. 11, pp. 6203–6212, Nov. 2015.

[35] I. Adam, "The load-reliant power transfer of the series-to-series inductive resonant wireless power transfer," *Test Eng. Manag.*, vol. 81, no. 5702, pp. 5702–5708, 2019.

[36] H. W. B. Roger C. Dugan, and M. F. McGranaghan, and S. Santoso, *Electrical Power Systems Quality*, 2017.

ISMAIL ADAM (Member, IEEE) received the B.Eng. degree (Hons.) from the University of Hertfordshire, the M.Sc. degree in electrical, electronics, and systems from the National University of Malaysia, and the Ph.D. degree in engineering from International Islamic University Malaysia, in 2021. He is currently a Senior Lecturer in the electronics section with UniKL BMI. With a strong presence in both teaching and research, his expertise spans wireless power transfer, sensors, transducers, embedded systems, and fuzzy logic control. He has authored and co-authored more than 50 articles and has been involved in significant projects, including the Power Line Data Communication Project and the Flexible Manufacturing System (FMS) Project. Since 2022, he has been an Electronics Engineering Consultant with the HEVTOL Project. He recognized as a National Industry Expert in industrial electronics since 2009, he has actively contributed to skill development and represented Malaysia with the ASEAN and World Skills Competitions.

MESHARI D. ALANAZI received the B.Sc. degree in electrical engineering (electronics and communications) from Jouf University, Saudi Arabia, the M.Sc. degree in electrical engineering from Bridgeport University, Bridgeport, CT, USA, in 2015, and the Ph.D. degree in electrical engineering from The University of Sheffield, Sheffield, U.K., in 2022. He is currently an Assistant Professor with the Department of Electrical Engineering, Jouf University. His research interests include antenna design and millimeter waves, microwave circuits, multiband antennae, filters, DRA, and others.

SHEROZ KHAN (Life Senior Member, IEEE) was born in Nawai-Wadana, Chārsadda, Khyber Pakhtunkhwa, Pakistan. He received the B.Sc. degree in electrical engineering from the N. W. F. P. University of Engineering and Technology (UET), Pakistan, in 1981, the M.Sc. degree in microelectronic and computer engineering from Surrey University, U.K., in 1990, and the Ph.D. degree from Strathclyde University, Glasgow, U.K., in 1994. He was a Principal Lecturer with UNITEN, from 2000 to 2001, an Associate Professor, and a Professor with the Department of ECE, International Islamic University Malaysia (IIUM), from 2002 to 2019. He has been the PG Coordinator of the ECE Department, IIUM, and the Founding Coordinator of the Wireless Communication and Signal Processing Research Group, from 2006 to 2019. He has been among the top 30 contributors to IIUM Research Performance, from 2019 and 2020. Since December 2019, he has been a Professor with the Department of Electrical Engineering, Onaizah College of Engineering and Information Technology, Saudi Arabia. He has been the Co-Founder of ICSIMA, ICISE, ICIRD, and ICETAS. He is currently the Founder of the IIUM-Limoges (France) and IIUM-Schmalkalden UAS (Germany) programs and has produced twenty-two (22) M.Sc. and ten (10) Ph.D., two (2) postdoctorate under his direct supervision while producing eight (8) Ph.D. under co-supervision. He is charged with the task of organizing webinars and international conferences alongside the department research committee chair. He is with the QU-IIUM-UniKL Research Team, KSA MoE RDO Grant Worth 1.277M SAR. He leads the Best Graduate Honor Board, Department of Electrical and Electronics Engineering, NWFP University of Engineering and Technology, Peshawar, Pakistan. He is a Senior Member of IEE, a Member of IET, and a C.Eng. He was awarded the Best Graduate University Scholarship for doing the M.Sc. degree. His ScienceDirect Scopus ID (7404043105) and Web-of-Science ID (ADU-0182-2022).

MASHKURI YAACOB (Senior Member, IEEE) received the Ph.D. degree from the University of Manchester, in 1980.

He was appointed as the Vice-Chancellor of UNITEN, in January 2007. Previously, he was the Deputy Vice-Chancellor (an Academic) of the University of Malaya (UM). He was the Founding Dean of the Computer Science and IT Faculty, UM. He is currently a Professor with the Computer and Electrical Department, Faculty of Engineering, UIAM, Malaysia. As the Vice-Chancellor, he has played a significant role in the growth of the university, particularly in rebranding the university as a Quality Private University, Malaysia.

Dr. Yaacob was a Council Member of IET, London, from 2003 to 2005. He was the Chairman of the Institution of Engineering and Technology (IET), Malaysia Branch, U.K. He initiated the publication of *Malaysian Journal of Computer Science*, in 1986, which has now received Thomson ISI recognition. UNITEN won the coveted Prime Minister's Industry Quality Excellence Award, in 2009, the International Asia Pacific Quality Award 2010 for Education, and the International Crown Quality Award 2010 for Education, London.

ANIS NURASHIKIN NORDIN (Senior Member, IEEE) received the B.Eng. degree in computer engineering from IIUM and the M.Sc. and Doctor of Science degrees in microelectronics and VLSI from The George Washington University, Washington, DC, USA, in 2003 and 2008, respectively. She has extensive international collaborative networks and was an Invited Researcher with Linkoping University, Sweden, the City College of New York, USA, Griffith University, Australia, and the University of Twente, Holland. She is currently a Microelectronics Professor and a Researcher with the Department of Electrical and Computer Engineering, (IIUM), Kuala Lumpur, Malaysia. She has been teaching courses in electronics engineering, since 2003. Her area of specialization is in the field of micro-electro-mechanical systems (MEMS). Upon completion of her Ph.D., she decided to work on developing biosensors that would reduce the pain burden of chemotherapy on patients. Her most innovative product to date is a personalized cancer chemotherapeutics kit, which can select the best chemotherapy drug for the patient and its optimum dosage. She has also developed numerous micro-sized devices, such as resonators and energy harvesters. Her novel innovations have been well received and have been awarded in both international and local exhibitions, such as IENA, Nuremberg, and British Invention Show, London. She holds two U.S. patents. Her work has been published both locally and internationally in more than 100 articles in journals and proceedings locally and internationally. She won the IIUM's Most Promising Researcher Award, in 2010, and the IIUM's Most Outstanding Researcher Award, in 2014.

MOHAMED HADI HABAEBI (Senior Member, IEEE) is currently a Professor with the Department of Electrical and Computer Engineering, International Islamic University Malaysia (IIUM). His research interests include the IoT, mobile app development, networking, AI applications in image processing, wireless communications, a small antenna, and channel propagation modeling. His WoS ID (P-2128-2017) and Scopus ID (6602298043).

HASMAH MANSOR (Senior Member, IEEE) received the B.Eng. degree (Hons.) in electronics and electrical engineering from the University of Salford, U.K., and the Master of Science and Ph.D. degrees in control and automation engineering from the University of Putra Malaysia. In January 2017, she was appointed as the Deputy Dean of Student Affairs, Faculty of Engineering, UIAM. Currently, she is an Associate Professor with the Electrical and Computer Engineering Department. Her research interests include instrumentation and control systems. She was awarded a Chartered Engineer, U.K., in January 2019.